



Treatment Strategy and Follow-up Evaluation for an Unruptured Anterior Communicating Artery Aneurysm Associated with Pseudo-Occlusion of the Internal Carotid Artery Using Computational Fluid Dynamics Simulations

Rüptüre Olmamış ve İnternal Karotid Arterin Psödooklüzyonuyla İlişkili Anterior Kominikan Arter Anevrizmasında Kompütasyonel Sıvı Dinamiği Simülasyonları Kullanılarak Tedavi Stratejisi ve Takip Değerlendirmesi

Kenichi KONO, Tomoaki TERADA

Wakayama Rosai Hospital, Department of Neurosurgery, Wakayama, Japan

Corresponding Author: Kenichi KONO / E-mail: vyr01450@gmail.com

ABSTRACT

Basic research on cerebral aneurysms using computational fluid dynamics (CFD) simulations has recently progressed. We describe a clinical case with the use of CFD simulations. A 76-year-old woman had an unruptured anterior communicating artery aneurysm associated with pseudo-occlusion of the internal carotid artery (ICA). Pre-operative CFD simulations demonstrated that carotid artery stenting (CAS) would decrease hemodynamic stress on the aneurysm and might reduce the risk of aneurysm rupture. We performed CAS, and did not surgically treat the aneurysm because of her advanced age. A 7-month follow-up angiogram showed no change in the aneurysm size. We performed CFD simulations using the patient-specific flow waveforms at the bilateral ICAs before and 7 months after CAS. Maximum time-averaged wall shear stress of the aneurysm decreased from 8.3 Pa to 4.4 Pa. The pressure loss coefficient of the aneurysm, a proposed hemodynamic value for rupture risk, increased from 1.83 to 2.75. These findings indicated that CAS might reduce the rupture risk of the aneurysm according to previous reports on CFD studies. The aneurysm remains unruptured for 14 months from the CAS. This is the first report to attempt to reduce the rupture risk of an unruptured aneurysm with flow alteration based on CFD simulations.

KEYWORDS: Cerebral aneurysm, Computational fluid dynamics simulations, Pseudo-occlusion, Rupture risk, Treatment strategy

ÖZ

Bilgisayarlı sıvı dinamiği (BSD) simülasyonları kullanılarak serebral anevrizmalar üzerinde temel araştırmalarda ilerlemeler olmuştur. BSD simülasyonları kullanımıyla bir klinik olguyu tanımlıyoruz. 76 yaşında bir kadında internal karotid arterin (İKA) psödooklüzyonuyla ilişkili rüptüre olmamış bir anterior kominikan arter anevrizması vardı. Preoperatif KSD simülasyonları karotid arter stentlemesinin (KAS) anevrizmadaki hemodinamik stresi azaltacağını ve anevrizma rüptürü riskini azaltmasının mümkün olduğunu ortaya koydu. KAS işlemi gerçekleştirdik ve yaşının ileri olması nedeniyle anevrizmayı cerrahi olarak tedavi etmedik. 7 ay sonra yapılan takip anjiyogramı anevrizma büyüklüğünde değişiklik olmadığını gösterdi. KAS'tan önce ve 7 ay sonra bilateral İKA'da hastaya spesifik akış dalgaformlarını kullanarak KSD simülasyonları yaptık. Anevrizmanın maksimum zaman aralıklı duvar kırpması stresi 8,3 Pa'dan 4,4 Pa'ya düştü. Rüptür riski için kullanımı önerilen bir hemodinamik değer olan anevrizma basınç kaybı katsayısı 1,83'ten 2,75'e arttı. Bu bulgular önceki KFS çalışmaları raporları temelinde KAS'ın anevrizma rüptür riskini azaltabileceğine işaret etti. Anevrizma KAS'tan 14 ay sonra halen rüptüre olmamış durumdadır. Bu rapor rüptüre olmamış bir anevrizmada KSD simülasyonları temelinde akış alterasyonu rüptür riskini azaltma girişimi açısından ilk rapordur.

ANAHTAR SÖZCÜKLER: Serebral anevrizma, Kompütasyonel sıvı dinamiği simülasyonları, Psödooklüzyon, Rüptür riski, Tedavi stratejisi

INTRODUCTION

Research on computational fluid dynamics (CFD) studies for cerebral aneurysms has recently rapidly progressed (3, 6). However, CFD simulations are still far from clinical application. We present a case of an unruptured anterior communicating

(Acom) aneurysm associated with pseudo-occlusion of the internal carotid artery (ICA). We used CFD simulations for designing a treatment strategy and follow-up evaluation. Our case could be one of the pioneer cases of clinical practice of CFD simulations.

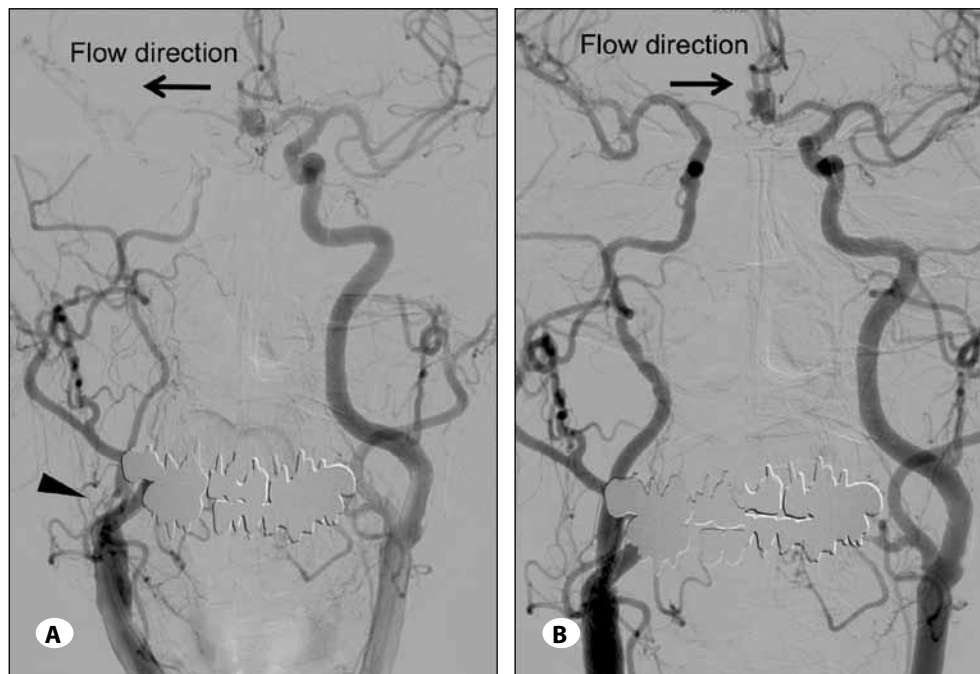


Figure 1: (A) Pre-operative angiogram. The bilateral carotid angiograms are fused. They show pseudo-occlusion at the right internal carotid artery (ICA) (arrow head), which collapses the distal portion of the right ICA. The left ICA angiogram shows an unruptured anterior communicating artery (Acom) aneurysm. The right middle cerebral territory is supplied from the left ICA via the Acom artery. The flow direction of the right A1 segment is from left to right (arrow). (B) Angiogram 7 months after the carotid artery stenting. The bilateral carotid angiograms are fused. The right middle cerebral territory is supplied from the right ICA. The flow direction of the right A1 segment is inverted (arrow).

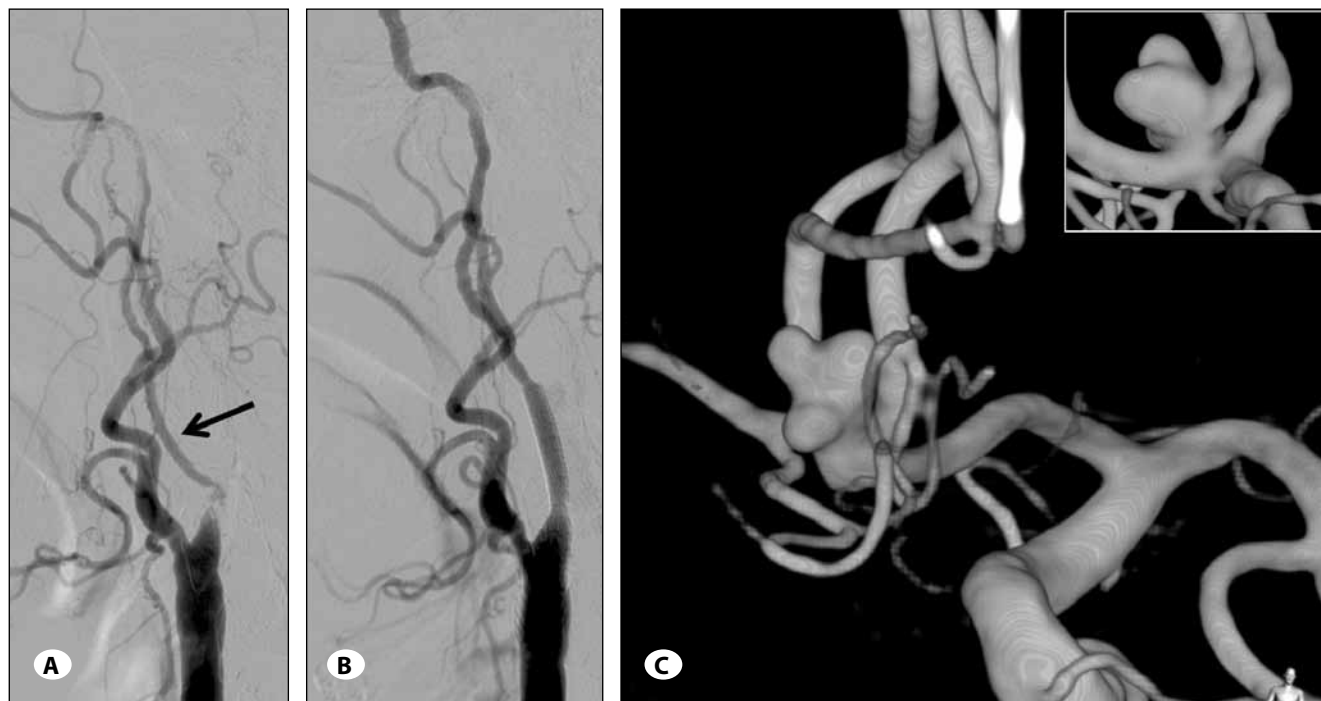


Figure 2: Lateral views of the right carotid angiogram before (A) and after (B) carotid artery stenting (CAS). The flow velocity at the right internal carotid artery before CAS was measured at the distal portion of the pseudo-occlusion (arrow) by carotid sonography. (C). Anterior-posterior view of a three-dimensional rotational angiogram shows a multi-lobulated, complex and wide-neck anterior communicating artery aneurysm. In the right upper window, the posterior-anterior view of the aneurysm is shown.

CASE REPORT

Clinical Presentation and Pre-Operative CFD Simulations

A 76-year-old woman presented with dizziness, and magnetic resonance imaging (MRI) revealed a 7-mm unruptured Acom aneurysm and pseudo-occlusion of the right ICA (Figures 1A, 2A,C). Although diffusion-weighted MRI showed no acute infarct, fluid attenuated inversion recovery MRI showed an old infarction of the right hemisphere. Therefore, we considered that the pseudo-occlusion was potentially symptomatic. Single photon emission tomography showed hemodynamic stage 1 based on Powers' classification. A left ICA angiogram showed the Acom aneurysm, the right A1 segment, and the right middle cerebral artery through the Acom artery because of low flow from the right ICA (Figure 1A). We had three options for designing a treatment strategy for the Acom aneurysm and the pseudo-occlusion. We could choose observation, clipping, or coil embolization with stent-assist for the Acom aneurysm. We could select medical treatment, carotid artery stenting (CAS), or carotid endarterectomy for the pseudo-occlusion. Stent-assist would be necessary for coil embolization because the aneurysm was wide-necked and complex (Figure 2C). To evaluate the hemodynamics around the Acom complex with the aneurysm, we performed pre-operative CFD simulations. Three-dimensional (3D) geometry of the aneurysm with the left ICA, the left A1 segment, and the right distal A1 segment was obtained by a 3D rotational angiogram. Because we could not obtain clear 3D geometry of the right ICA and the proximal portion of the right A1 segment, we created an aneurysm model with the bilateral ICA by flipping and fusion of the left ICA geometry using 3-matic software (Materialise NV, Leuven, Belgium). We used an implicit solver, ANSYS CFX (Version 14.0, ANSYS Inc.) for the CFD simulations. The detailed methods and validation study were described previously (7, 8, 13). The number of elements was approximately 800,000. The mean flow velocity at the left ICA by ultrasonography was 0.34 m/sec in this

patient. To clarify hemodynamic flow patterns around the aneurysm, we performed steady flow simulations imposing 0.34 m/sec constant inlet flow only at the right ICA (Figure 3A), only at the left ICA (Figure 3B), or at the bilateral ICA (Figure 3C). Although these were steady flow simulations and the right ICA geometry was not real, we considered that they were sufficient to show global flow patterns around the Acom aneurysm. These simulations demonstrated that the flow from the left A1 segment predominantly entered the aneurysm compared with the flow from the right A1 segment (Figure 3A-C). Without the CFD simulations, it was difficult to determine these flow patterns because of the complex Acom structure in this patient (Figure 2C). According to the CFD results, we considered that pseudo-occlusion of the right ICA increased the amount of flow of the left A1 segment (Figure 1A), which might increase the risk of aneurysm rupture. Therefore, we postulated that resolving the pseudo-occlusion by CAS would decrease flow rate at the left A1 segment and might decrease the risk of aneurysm rupture. In addition, considering our patient's advanced age (76 years old), surgical aneurysm treatment, such as clipping or stent-assisted coil embolization, appeared to be too aggressive.

We performed CAS for the pseudo-occlusion using a flow reversal system (Figure 2B) (9). The patient was discharged with no complications. We performed a follow-up angiogram 7 months after CAS. The angiogram showed expansion of the whole segment of the right ICA. The flow direction of the right A1 segment was inverted (Figure 1B). The angiogram also showed no change in size and shape of the aneurysm. The patient remained neurologically intact and the aneurysm stayed unruptured for 14 months from CAS.

Post-Operative CFD Simulations and Evaluation of the Rupture Risk

To evaluate changes in the rupture risk during the 7 months, we performed CFD simulations using patient-specific flow waveforms. We performed time series carotid ultrasonography and measured flow velocity and the cross-sectional area

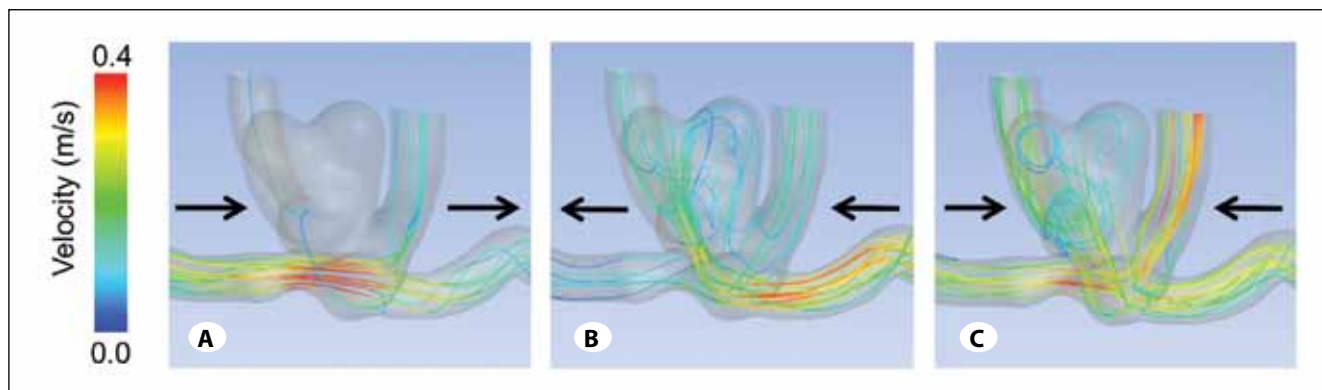


Figure 3: Pre-operative computational fluid dynamics (CFD) simulations. Streamlines are shown in three different inlet conditions: **(A)** Constant flow only at the right internal carotid artery (ICA), **(B)** only at the left ICA, and **(C)** at the bilateral ICA. Arrows indicate flow direction in all panels. **(A)** There is little flow from the right A1 segment entering the aneurysm. **(B)** A lot of flow from the left A1 segment enters the aneurysm, indicating that flow into the aneurysm predominantly comes from the left A1 segment.

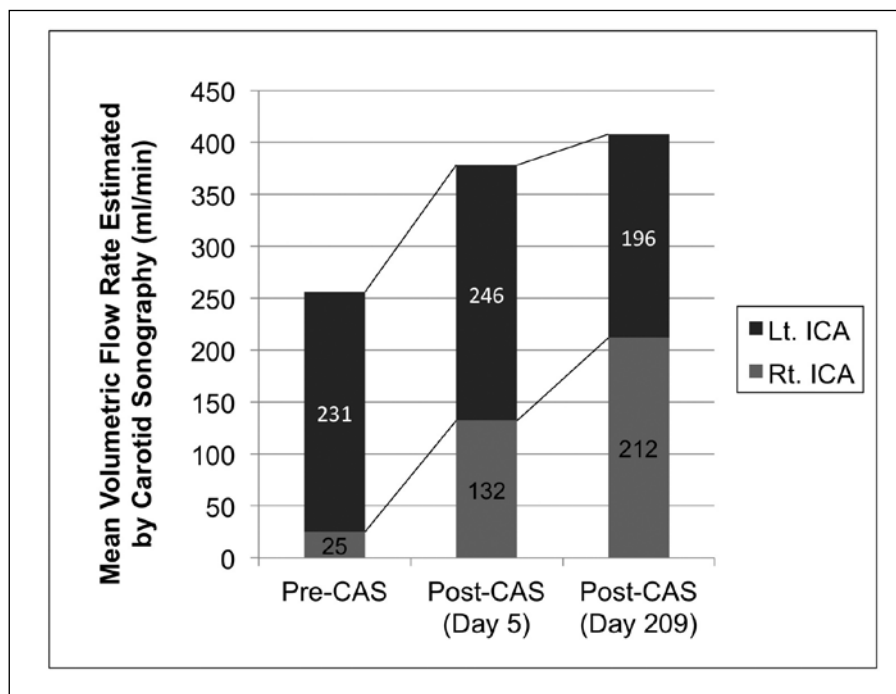


Figure 4: Measurement of mean volumetric flow rates by carotid sonography. Mean flow velocity and the cross-sectional area of the bilateral internal carotid arteries (ICAs) were measured by carotid sonography. The flow rates were measured before CAS, and 5 days or 209 days after CAS. The flow rate at the right ICA was increased, while the flow rate at the left ICA was decreased after CAS. Rt.: right, Lt.: left.

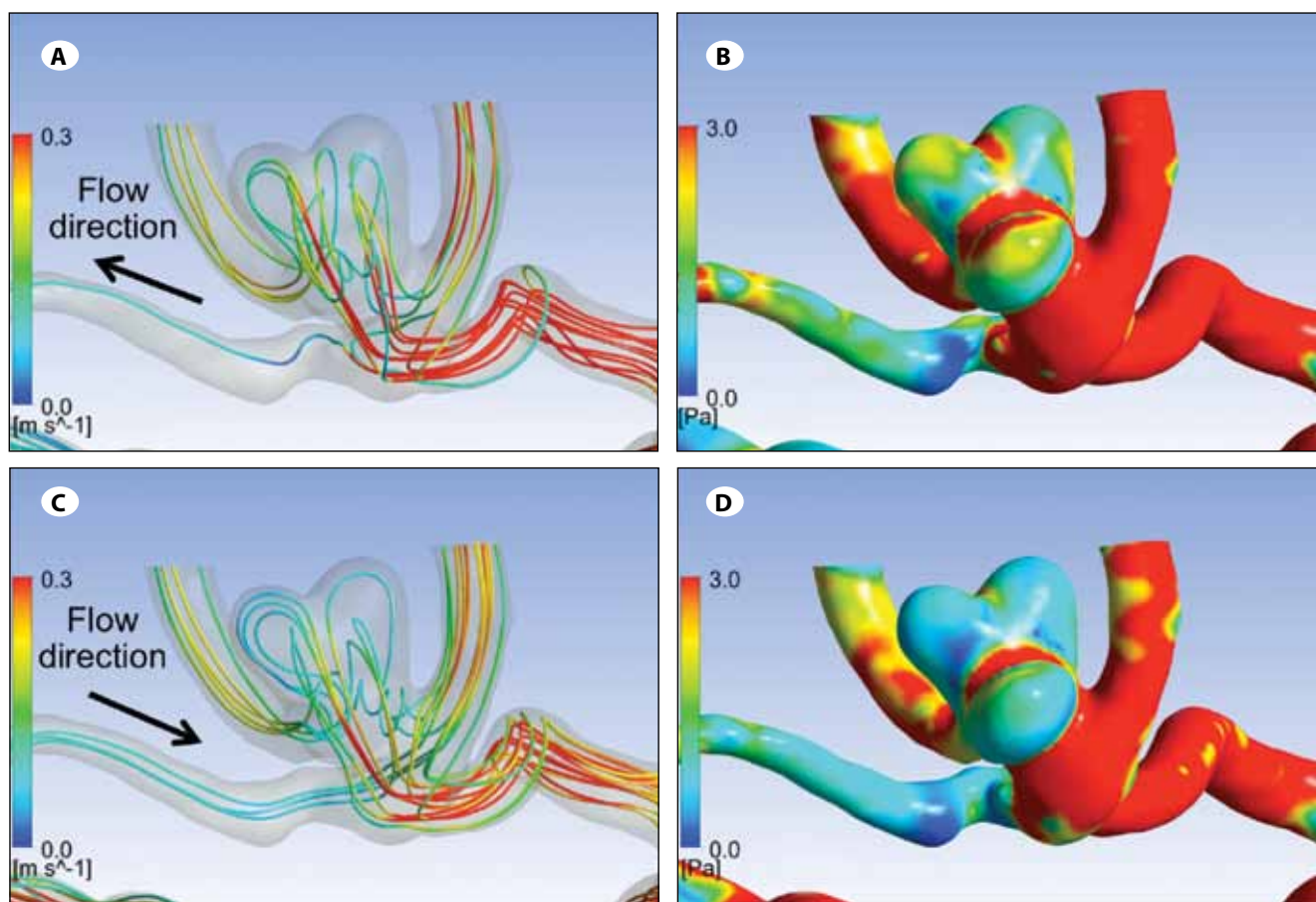


Figure 5: Computational fluid dynamics simulations show peak systolic streamlines colored according to velocity (A and C) and the contour of wall shear stress (WSS) (B and D) using the patient-specific flow waveforms before (A and B) and 7 months after the operation (C and D). The flow direction of the right A1 segment was left to right before the operation (arrow in A) and right to left after the operation (arrow in C), which is consistent with angiographic results.

Table I: Hemodynamic Values of the Aneurysm before and after Carotid Artery Stenting

Time	PLc	Maximum TAWSS (Pa)	Area-averaged TAWSS (Pa)
Pre-CAS	1.83	8.3	1.26
Post-CAS (day 209)	2.75	4.4	0.42

CAS: carotid artery stenting, **PLc:** pressure loss coefficient, **TAWSS:** time-averaged wall shear stress.

at the bilateral ICAs before, and 5 and 209 days (7 months) after CAS. Before CAS, the flow velocity and cross-sectional area at the right ICA were measured at the distal portion of the pseudo-occlusion (Figure 2A). The mean flow velocity was multiplied by the cross-sectional area to calculate the mean volumetric flow rate. The flow rate at the right ICA was increased, while the flow rate at the left ICA was decreased (Figure 4), as expected.

We fused two 3D geometries obtained by a follow-up 3D rotational angiogram of the right or left ICA. For inlet conditions, we used patient-specific volumetric flow waveforms of the bilateral ICAs before and 7 months after CAS. We performed pulsatile CFD simulations, which have been previously described in detail (7, 10). The number of elements was approximately 730,000. When observing the streamlines, the flow direction of the right A1 segment was from left to right before CAS and right to left after CAS (Figure 5A, C). This was consistent with the angiographic results (Figure 1A,B), validating the CFD simulations. We measured the pressure loss coefficient (PLc) of the aneurysm (14), maximum time-averaged wall shear stress (TAWSS) on the aneurysm, and area-averaged TAWSS on the aneurysm (Table I). This was performed because low PLc (14), high maximum TAWSS (2, 4), and low area-averaged TAWSS (12, 15), are reported to be associated with ruptured aneurysms. After CAS, the PLc was increased, while the maximum TAWSS and the area-averaged TAWSS were decreased (Table I). Elevated PLc and decreased maximum TAWSS suggested that the rupture risk of the aneurysm might be decreased (2, 4, 14). However, decreased area-averaged TAWSS implied that the rupture risk of the aneurysm might be increased (12, 15). Although this appeared to be a contradiction, we considered that the rupture risk was decreased for the following reasons. First, in previous studies of wall shear stress (WSS) (2, 4, 12, 15), unruptured aneurysms were compared with already ruptured aneurysms. The geometry of ruptured aneurysms might change after rupture. Therefore, these previous results may not be used for prediction of the rupture risk of unruptured aneurysms. A study on the PLc (14) compared unruptured aneurysms that stayed unruptured with those that eventually ruptured, and concluded that unruptured aneurysms with a low PLc have a significantly higher risk of rupture. Therefore, the PLc may be superior to predict the rupture risk of unruptured aneurysms. Second, the findings of high maximum TAWSS (2, 4) and low area-averaged TAWSS (12, 15) appear to contradict each other. We cannot determine which is correct. Based on clinical reports, increased hemodynamic stress appears to increase the risk of aneurysm rupture (1,

5,11). Because an increase in flow velocity will elevate WSS, it is reasonable to consider that elevated WSS may increase the rupture risk. Therefore, we consider that elevated maximum TAWSS is a more predominant predictor of rupture risk than lowered area-averaged WSS. Consequently, we consider that CAS alters flow distribution and might decrease the risk of aneurysm rupture as we had expected before treatment (Figure 5B, D).

DISCUSSION

In this case report, we used CFD simulations for designing a treatment strategy and evaluating the change in rupture risk after CAS. Before treatment, we could not predict how much the flow rate at the ICAs CAS would change. Therefore, we performed steady CFD simulations for designing a treatment strategy. To evaluate the rupture risk, we measured the volumetric flow rate at the bilateral ICAs using carotid sonography. We could then perform pulsatile CFD simulations using the time series of patient-specific flow waveforms and compare hemodynamic values before and after CAS. With this combination of CFD simulations, we were able to use CFD simulations for designing a treatment strategy and follow-up evaluation as a clinical application. Although a long follow-up of the patient is necessary, this could be a pioneer case of clinical application of CFD simulations.

Several CFD reports have proposed that hemodynamic values are associated with aneurysm rupture, such as low area-averaged TAWSS (12, 15), high maximum TAWSS (2, 4), and a low PLc (14). However, it is difficult to use these values for clinical application because of two reasons. First, there are no clear absolute thresholds of these hemodynamic values. Second, different CFD solvers under different conditions will yield different absolute hemodynamic values, although a comparative relationship may be maintained (13). Therefore, it is difficult to use these hemodynamic values for predicting the rupture risk. However, we may overcome these two problems if we evaluate these values in the same patient. For example, these values may be used to predict the ruptured side in two mirror image aneurysms (8). The current case is another clinical application. Namely, flow alterations changed hemodynamic values of the aneurysm, which we could compare before and after treatment. In both cases, we do not need to evaluate absolute hemodynamic values but just compare them.

We appreciate that there are several limitations to our CFD simulations, as we have previously stated (7, 8, 10). In particular, in this case, we could not obtain and use the 3D geometry of the pseudo-occlusion of the right ICA. The geometry of the

right ICA was changed after CAS, which we could not take into consideration in our CFD simulations. However, we consider that our CFD analysis is still valid because we compared hemodynamic values under the different inlet conditions and did not depend on the absolute values. This comparison may be relatively robust, although we cannot estimate how much annual rupture risk we could actually decrease in this patient.

REFERENCES

1. Briganti F, Cirillo S, Caranci F, Esposito F, Maiuri F: Development of "de novo" aneurysms following endovascular procedures. *Neuroradiology* 44:604-609, 2002
2. Castro MA, Putman CM, Sheridan MJ, Cebra JR: Hemodynamic patterns of anterior communicating artery aneurysms: A possible association with rupture. *AJNR Am J Neuroradiol* 30:297-302, 2009
3. Cebra JR, Meng H: Counterpoint: Realizing the clinical utility of computational fluid dynamics - closing the gap. *AJNR Am J Neuroradiol* 33:396-398, 2012
4. Cebra JR, Mut F, Weir J, Putman C: Quantitative characterization of the hemodynamic environment in ruptured and unruptured brain aneurysms. *AJNR Am J Neuroradiol* 32:145-151, 2011
5. Jin SC, Choi CG, Kwon DH: Development of 'De novo' aneurysm after therapeutic carotid occlusion. *J Korean Neurosurg Soc* 45:236-239, 2009
6. Kallmes DF: Point: CFD - computational fluid dynamics or confounding factor dissemination. *AJNR Am J Neuroradiol* 33:395-396, 2012
7. Kono K, Fujimoto T, Shintani A, Terada T: Hemodynamic characteristics at the rupture site of cerebral aneurysms: A case study. *Neurosurgery* 71:E1202-E1209, 2012
8. Kono K, Shintani A, Fujimoto T, Terada T: Stent-assisted coil embolization and computational fluid dynamics simulations of bilateral vertebral artery dissecting aneurysms presenting with subarachnoid hemorrhage: Case report. *Neurosurgery* 71:E1192-E1201, 2012
9. Kono K, Tanaka Y, Yoshimura R, Fujimoto T, Okada H, Shintani A, Terada T: Emergent carotid artery stenting using a flow reversal system for acute atherosclerotic occlusion of the internal carotid artery. *Acta Neurochir (Wien)* 153:2175-2180, 2011
10. Kono K, Terada T: Hemodynamics of 8 different configurations of stenting for bifurcation aneurysms. *AJNR Am J Neuroradiol* 1-7, 2013
11. Otawara Y, Ogasawara K, Ogawa A, Kogure T: Dissecting aneurysms of the bilateral vertebral arteries with subarachnoid hemorrhage: Report of three cases. *Neurosurgery* 50:1372-1374; discussion 1374-5, 2002
12. Shojima M, Oshima M, Takagi K, Torii R, Hayakawa M, Katada K, Morita A, Kirino T: Magnitude and role of wall shear stress on cerebral aneurysm: Computational fluid dynamic study of 20 middle cerebral artery aneurysms. *Stroke* 35:2500-2505, 2004
13. Steinman D, Hoi Y, Fahy P, Morris L, Walsh M, Aristokleous N, Anayiotos A, Papaharilaou Y, Arzani A, Shadden S, Berg P, Janiga G, Bols J, Segers P, Bressloff N, Cibis M, Gijssen F, Cito S, Pallarés J, Browne L, Costelloe J, Lynch A, Degroote J, Vierendeels J, Fu W, Qiao A, Hodis S, Kallmes D, Kalsi H, Long Q, Kheyfets V, Finol E, Kono K, Malek A, Lauric A, Menon P, Pekkan K, Moghadam M, Marsden A, Oshima M, Katagiri K, Peiffer V, Mohamied Y, Sherwin S, Schaller J, Goubergrits L, Usera G, Mendina M, Valen-Sendstad K, Habets D, Xiang J, Meng H, Yu Y, Karniadakis G, Shaffer N, Loth F: Variability of CFD solutions for pressure and flow in a giant aneurysm: The SBC2012 CFD challenge. *J Biomech Eng* 135(2):1-13, 2013
14. Takao H, Murayama Y, Otsuka S, Qian Y, Mohamed A, Masuda S, Yamamoto M, Abe T: Hemodynamic differences between unruptured and ruptured intracranial aneurysms during observation. *Stroke* 43:1436-1439, 2012
15. Xiang J, Natarajan SK, Tremmel M, Ma D, Mocco J, Hopkins LN, Siddiqui AH, Levy EI, Meng H: Hemodynamic-morphologic discriminants for intracranial aneurysm rupture. *Stroke* 42:144-152, 2011